

THE ANALYSIS OF π^- MESONS PRODUCED IN NUCLEUS-NUCLEUS
COLLISIONS AT A MOMENTUM OF 4.5 GeV/c/NUCLEON IN LIGHT
FRONT VARIABLES

M.Anikina^a, L.Chkhaidze^b, T.Djobava^b,
V.Garsevanishvili^c, L.Kharkhelaury^b

^a *Joint Institute for Nuclear Research, 141980 Dubna, Russia*

^b *High Energy Physics Institute, Tbilisi State University,
University Str. 9, 380086 Tbilisi, Republic of Georgia*

^c *Mathematical Institute of the Georgian Academy of Sciences
M.Alexidze Str. 1, 380093 Tbilisi, Republic of Georgia*

E-mail: djobava@sun20.hepi.edu.ge

ABSTRACT

The light front analysis of π^- mesons in He(Li,C), C-Ne, C-Cu and O-Pb collisions is carried out. The phase space of secondary pions is divided into two parts in one of which the thermal equilibrium assumption seems to be in a good agreement with the data. Corresponding temperatures T are extracted and their dependence on $(A_P * A_T)^{1/2}$ is studied. The results are compared with the predictions of the Quark-Gluon String Model (QGSM). The QGSM satisfactorily reproduces the experimental data for light and intermediate-mass nuclei.

PACS: 25.70.-z

Keywords: NUCLEAR REACTION He(Li, π^- ,X), He(C, π^- ,X), C(Ne, π^- ,X), C(Cu, π^- ,X), O(Pb, π^- ,X) at 4.5 GeV/c/nucleon; measured pion distributions: deduced thermal equilibrium, characterized by the temperature T . Analysis in light-front variables. Comparison with the Quark Gluon String Model. Light-front variables; Phase space; Thermal equilibrium.

1. INTRODUCTION

In the present paper we continue the study of π^- mesons produced in the relativistic nucleus-nucleus collisions in terms of the light front variables. The choice of the light front variables is due to the fact, that these variables seem to be more sensitive to the dynamics of interaction as compared to the well-known Feynman variables x_F and rapidity Y .

In the previous publication [1] we performed the light front analysis of π^- mesons produced in Mg-Mg collisions at 4.3 GeV/c. On the basis of this analysis we were able to separate the region of the phase space, where the thermal equilibrium seems to be reached. It is interesting in this connection to perform the same analysis for other pairs of nuclei (He(Li,C), C-Ne, C-Cu, O-Pb) in order to study the dependence of the corresponding characteristics on the atomic number of colliding pairs of nucleus . The data were obtained on the SKM-200-GIBS facility of the Dubna Joint Institute for Nuclear Research.

2. EXPERIMENT

SKM-200-GIBS consists of a 2m streamer chamber, placed in a magnetic field of ~ 0.8 T and a triggering system. The streamer chamber was exposed by beams of He , C , O , Ne and Mg nuclei accelerated in the synchrophasotron up to a momentum of 4.5 GeV/c per incident nucleon. The solid targets in the form of thin discs with thickness $0.2 \div 0.4$ g/cm² (for Li the thickness was 1.59 g/cm² and for Mg 1.56 g/cm²) were mounted within the fiducial volume of the chamber. Neon gas filling of the chamber served also as a nuclear target. The triggering system allowed the selection of "inelastic" and "central" collisions.

The central trigger was selecting events with no charged and neutral projectile spectator fragments (with $P/Z > 3$ GeV/c) within a cone of half angle Θ_{ch} , $\Theta_n = 2^0$ or 3^0 . The trigger mode for each exposure is defined as T (Θ_{ch} , Θ_n). Thus T(0,0) corresponds to all inelastic collisions. For inelastic collisions He-Li and He-C all charged secondaries were measured and central subsamples T(2,0) were selected. The details of the experimental setup and the logic of the triggering systems are presented in [1,2].

Primary results of scanning and measurements were biased due to several experimental effects and appropriate corrections were introduced. The biases and correction procedures were discussed in detail in [2,3]. Average measurement errors of the momentum and production angle determination for π^- mesons were $< \Delta P/P > = 5\%$, $\Delta\Theta = 0.5^0$ for He-Li, He-C, C-Ne, C-Cu, O-Pb.

3. THE DATA ANALYSIS IN TERMS OF THE LIGHT FRONT VARIABLES

The light front variables ξ^\pm in the centre of mass frame for the inclusive reaction $a + b \rightarrow c + X$ are defined as follows [1]:

$$\xi^\pm = \pm \frac{E \pm p_z}{\sqrt{s}} = \pm \frac{E + |p_z|}{\sqrt{s}} \quad (1)$$

where s is the usual Mandelstam variable, $E = \sqrt{p_z^2 + p_T^2 + m^2}$ and p_z are the energy and the z - component of the momentum of produced particle. The z -axis is taken to be the collision axis i.e. $p_z = p_3$. The upper sign in Eq. (1) is used for the right hand side hemisphere and the lower sign for the left hand side hemisphere. In order to enlarge the scale in the region of small ξ^\pm , it is convenient also to introduce the variables

$$\zeta^\pm = \mp \ln |\xi^\pm| \quad (2)$$

The invariant differential cross section in terms of these variables looks as follows:

$$E \frac{d\sigma}{d\vec{p}} = \frac{|\xi^\pm|}{\pi} \frac{d\sigma}{d\xi^\pm dp_T^2} = \frac{1}{\pi} \frac{d\sigma}{d\zeta^\pm dp_T^2} \quad (3)$$

The light front variables have been introduced by Dirac [4] and they are widely used now in the treatment of many theoretical problems (see, e.g. original and review papers [5-10]).

The analysis has been carried out for the π^- mesons from He(Li,C), C-Ne, C-Cu and O-Pb collisions in the nucleus-nucleus centre of mass system.

The number of events for all pairs of nuclei and corresponding trigger modes are listed in Table 1. Due to the small statistics and average multiplicities, the data of He-Li and He-C collisions has been united and thus He(Li,C) represents this sample of the data. In Fig. 1 the ξ^\pm - distributions of π^- mesons from He(Li,C), C-Ne, C-Cu and O-Pb interactions are presented. These distributions are similar for all analysed pairs of nuclei. The principal differences of ξ^\pm distributions as compared to the corresponding x_F - distributions (Fig. 2) are the following: (1) existence of some forbidden region around the point $\xi^\pm = 0$; (2) existence of maxima at some $\tilde{\xi}^\pm$ in the region of relatively small $|\xi^\pm|$.

The experimental data for invariant distributions $(1/\pi) \cdot dN/d\zeta^\pm$ are shown in Fig. 3. The curves are the result of the polynomial approximation of the experimental distributions. The maxima at $\tilde{\zeta}^\pm$ are also observed in the invariant distributions $(1/\pi) \cdot dN/d\zeta^\pm$.

However, the region $|\xi^\pm| > |\tilde{\xi}^\pm|$ goes over to the region $|\xi^\pm| < |\tilde{\xi}^\pm|$ and vice versa (see Eqs. (1) and (2)). The value of maxima are observed at $\tilde{\zeta}^\pm = 2.0 \pm 0.1$ for all pairs of nuclei. The $\tilde{\zeta}^\pm$ is the function of the energy (see Eqs. (1), (2)) and does not depend on the mass numbers of the projectile (A_P) and target (A_T).

In order to study the nature of these maxima we have divided the phase space into two regions $|\zeta^\pm| > |\tilde{\zeta}^\pm|$ ($\tilde{\zeta}^+ = 2.0$) and $|\zeta^\pm| < |\tilde{\zeta}^\pm|$ and studied the p_T^2 and the angular distributions of π^- mesons in these regions separately. The numbers of pions in these two regions are approximately equal. For example in C-Cu interactions in the region $|\zeta^\pm| > |\tilde{\zeta}^\pm|$ the number of pions is equal to 1987 and in $|\zeta^\pm| < |\tilde{\zeta}^\pm|$ — 2212. In Figs. 4, 5 the p_T^2 and the angular distributions of π^- mesons from He(Li,C), C-Ne, C-Cu and O-Pb interactions in different regions of ζ^+ ($\zeta^+ > \tilde{\zeta}^+$ and $\zeta^+ < \tilde{\zeta}^+$) in the forward hemisphere are presented.

One can see from Figs. 4, 5, that the p_T^2 and the angular distributions of π^- mesons differ significantly in $\zeta^+ > \tilde{\zeta}^+$ and $\zeta^+ < \tilde{\zeta}^+$ regions. The angular distribution of pions in the region $\zeta^+ < \tilde{\zeta}^+$ (Figs. 5.b and 5.c) is sharply anisotropic in contrast to the almost flat distribution in the region $\zeta^+ > \tilde{\zeta}^+$ (Figs. 5.a and 5.c). The flat behaviour of the angular distribution allows one to think that one observes a partial thermal equilibrium [11] in the region $|\zeta^\pm| > |\tilde{\zeta}^\pm|$ ($|\xi^\pm| < |\tilde{\xi}^\pm|$) of phase space. The slopes of p_T^2 – distributions differ greatly in different regions of ζ^\pm (Fig. 4). Thus the values of $\tilde{\zeta}^\pm$ are the boundaries of the two regions with significantly different characteristics of π^- mesons. The validity of this statement can be seen from the momentum distributions of π^- mesons in the Laboratory frame. Fig. 6 presents the momentum distribution of pions from C-Cu collisions in the laboratory frame. The shaded area corresponds to the region of $\zeta^+ > \tilde{\zeta}^+$ and the non-shaded one to the region of $\zeta^+ < \tilde{\zeta}^+$. One can see from the Fig. 6, that these two regions almost do not overlap in the momentum space unlike to the cms case (overlap $\sim 45\%$). The pions from the region $\zeta^+ > \tilde{\zeta}^+$ have small momentum, approximately up to 0.6 GeV/c as compared to the pions from $\zeta^+ < \tilde{\zeta}^+$ (the momentum of pions ranges from ~ 0.6 GeV/c to 3 GeV/c). The similar results have been also obtained for the other pairs of nuclei. Fig. 7 presents the dependence of $\langle P \rangle_{lab}$ on Θ_{lab} for all analysed pairs of nuclei (He(Li,C) and C-Ne data are presented with the same symbol because of the similarity of their dependences) and Mg-Mg interactions in the $\zeta^+ > \tilde{\zeta}^+$ and $\zeta^+ < \tilde{\zeta}^+$ regions. The shapes of these dependences are different in two regions of ζ^+ . The curves are the result of polynomial approximation. $\langle P \rangle_{lab}$ decreases and $\langle \Theta \rangle_{lab}$ increases with the increasing of A_P , A_T .

To describe the spectra in the region $\zeta^+ > \tilde{\zeta}^+$ the Boltzmann

$$f(E) \sim e^{-E/T}$$

distribution have been used.

The distributions $1/\pi \cdot dN/d\zeta^+$, dN/dp_T^2 , $dN/d\cos\Theta$ look in this region as follows :

$$\frac{1}{\pi} \frac{dN}{d\zeta^+} \sim \int_0^{p_{T,max}^2} E f(E) dp_T^2 \quad (4)$$

$$\frac{dN}{dp_T^2} \sim \int_0^{p_{z,max}} f(E) dp_z \quad (5)$$

$$\frac{dN}{d\cos\theta} \sim \int_0^{p_{max}} f(E) p^2 dp \quad (6)$$

$$E = \sqrt{\vec{p}^2 + m_\pi^2}, \quad \vec{p}^2 = p_z^2 + p_T^2 \quad (7)$$

where:

$$p_{T,max}^2 = (\xi^+ \sqrt{s})^2 - m_\pi^2$$

$$p_{z,max} = [p_T^2 + m^2 - (\xi^+ \sqrt{s})^2] / (-2\xi^+ \sqrt{s})$$

$$p_{max} = (-\xi^+ \sqrt{s} \cos\Theta + \sqrt{(\xi^+ \sqrt{s})^2 - m_\pi^2 \sin^2\Theta}) / \sin^2\Theta$$

The experimental distributions in the region $\zeta^+ > \tilde{\zeta}^+$ have been fitted by the expressions (4), (5), (6), respectively. The results of the joint fit of the distributions $1/\pi \cdot dN/d\zeta^+$, dN/dp_T^2 , $dN/d\cos\Theta$ are given in Table 1 and Figs. 4, 5, 8. They show a rather good agreement with experiment. In Table 1 the values of the parameter T obtained by fitting the data with Boltzmann distribution are presented. In order to determine how the characteristics vary the analysis have been carried out also for $\tilde{\zeta}^+=1.9$ and 2.1 . The results are similar, but the joint fit of the distributions is better for $\tilde{\zeta}^+=2.0$ (presented on Figures).

The spectra of π^- mesons in the region $\zeta^+ > \tilde{\zeta}^+$ are satisfactorily described by the formulae which follow from the thermal equilibrium. The same formulae when extrapolated to the region $\zeta^+ < \tilde{\zeta}^+$ (Fig. 8) deviate significantly from the data. Therefore in the region $\zeta^+ < \tilde{\zeta}^+$ the p_T^2 - distributions has been fitted by the formula

$$\frac{dN}{dp_T^2} \sim \alpha \cdot e^{-\beta_1 p_T^2} + (1 - \alpha) \cdot e^{-\beta_2 p_T^2} \quad (8)$$

and the ζ^+ - distributions by the formula

$$\frac{1}{\pi} \cdot \frac{dN}{d\zeta^+} \sim (1 - \xi^+)^n = (1 - e^{-|\zeta^+|})^n \quad (9)$$

which is an analogue of the $(1 - x_F)^n$ dependence – the result of the well-known quark-parton model consideration (see, e.g. [12]), which for π^- mesons gives the value $n=3$. The dependence $(1 - e^{-|\zeta^+|})^n$ is in good agreement with experiment in the region $\zeta^+ < \tilde{\zeta}^+$ and

deviates from it in the region $\zeta^+ > \tilde{\zeta}^+$ (Fig. 8). The results of the fit are given in Table 1 and Figs. 4 and 8.

Thus in the ζ^\pm (ξ^\pm) distributions we have singled out points $\tilde{\zeta}^\pm$ ($\tilde{\xi}^\pm$) which separate in the phase space two groups of particles with significantly different characteristics. There are no such points in the x_F and Y - distributions.

In this paper the Quark Gluon String Model (QGSM) [13] is used for a comparison with experimental data. The QGSM is based on the Regge and string phenomenology of particle production in inelastic binary hadron collisions [14]. The QGSM simplifies the nuclear effects (neglects the potential interactions between hadrons, Pauli blocking, coalescence of nucleons and etc.) and concentrates on hadron rescatterings. The QGSM includes only low lying vector mesons and baryons with spin 3/2, mostly Δ (3/2, 3/2) resonances. A detailed description and comparison of the QGSM with experimental data in a wide energy range can be found in Ref. [1,15,16].

We have generated He(Li,C), C-Ne, C-Cu, O-Pb interactions using Monte-Carlo generator COLLI, based on the QGSM. The events had been traced through the detector and trigger filter.

In the generator COLLI there are two possibilities to generate events: 1) at not fixed impact parameter \tilde{b} and 2) at fixed b . The events have been generated for \tilde{b} . From the impact parameter distribution we obtained the mean value of $\langle b \rangle$. For the obtained value of $\langle b \rangle$, we have generated a total samples of $A_P - A_T$ events. The numbers of generated events for all analysed pairs of nuclei are listed in Table 1. The two regimes are consistent and it seems, that in our experiment the following values of b are most probable: $b=1.55$ fm for He(Li,C); $b=2.20$ fm for C-Ne; $b=2.75$ fm for C-Cu; $b=3.75$ fm for O-Pb.

The experimental results have been compared with the predictions of the QGSM for the above mentioned values of b and satisfactory agreement between the experimental data and the model have been found. In Figs 1.b and 3.b the ξ^\pm and ζ^\pm - distributions of π^- mesons from the QGSM calculations are presented together with the experimental ones for C-Cu interactions. One can see, that the QGSM reproduces these distributions well. The similar results have been obtained for all analysed pairs of nuclei. The QGSM also reproduces the p_T^2 and $\cos\Theta$ distributions (Figs. 4.c and 5.c). The QGSM data show the similar characteristics in the different regions of ζ as experimental ones: sharply anisotropic angular distributions in the region $\zeta^+ < \tilde{\zeta}^+$ and the almost flat distribution in the region $\zeta^+ > \tilde{\zeta}^+$; the slopes of p_T^2 - distributions differ greatly in different regions of ζ^+ ; the momentum distributions of pions in the laboratory frame in different regions of ζ^+ have the similar different shape of spectra as experimental ones (Fig 6). Momentum

distributions of QGSM data reproduces the corresponding experimental spectra in both regions of ζ^+ . The distributions obtained by the QGSM in the region $\zeta^+ > \tilde{\zeta}^+$ have been fitted by the expressions (4), (5), (6). The results of the fit are given in Table 1 and Figs. 4.c, 5.c. In the region $\zeta^+ < \tilde{\zeta}^+$ the p_T^2 and the ζ^+ – distributions have been fitted by the formulae (8) and (9), respectively. The results of the fit are given in Table 1 and Fig. 4.c. One can see from the Table 1, that the values of the T extracted from the experimental and QGSM data coincide within the errors. The QGSM does not reproduce satisfactorily the O-Pb data. This is may be caused by the fact, that QGSM simplifies the nuclear effects, which are more pronounced for heavy nuclei. In Ref. [17] it has been indicated that the model can be improved by including higher mass baryon resonances and taking into account a possible increase of the pion absorption cross section, $\sigma_{\Delta\Delta\rightarrow NN}$ in dense baryon medium, in comparison with the cross section, obtained from detailed balance relation.

In Fig. 9 the dependence of the parameter T from the Table 1 on $(A_P * A_T)^{1/2}$, obtained from the experimental and QGSM data, is presented. The temperature for Mg-Mg interactions is extracted from [1]. One can see, that T decreases linearly with the increasing of $(A_P * A_T)^{1/2}$ i.e with the increasing number of participating nucleons. Similar behaviour is predicted by the QGSM.

In our previous article [18] the temperatures of pions in He-Li, He-C, C-Ne, C-Cu and O-Pb interactions were obtained by means of inclusive kinetic energy and transverse momentum spectra in central rapidity interval (0.5 – 2.1 for light nuclei and 0.1 – 1.8 for heavy ones), which corresponds to the pionization region and with the c.m.s. angles $90^\circ \pm 10^\circ$. The pion spectra for He-Li, He-C and C-Ne have been fitted by one exponent and for C-Cu and O-Pb by a sum of two exponents, or two temperatures T_1 and T_2 (describing the low and high momentum part of the spectrum). The temperatures extracted by the light front analysis for light pairs of nuclei are less about (15–20) % as compared to those obtained in Ref. [18]. For heavy pairs of nuclei the temperatures are more close to the low temperature T_1 . It seems obvious, as the thermal equilibrium region corresponds to lower momenta. It should be mentioned that the extraction procedures of T in the light-front variables and in Ref. [18] are quite different and it seems, that different regions of phase space are separated by these two methods.

It is interesting to compare the temperatures extracted by means of light front analysis with those obtained in the GSI experiments (FOPI, KAON and TAPS- Collaborations, see, e.g. [19,20]). The T in the GSI experiments have been obtained in a same manner as in our Ref. [18]. The numerical values of the parameter T for pions in Au-Au collisions at 1 A GeV and our values for heaviest colliding pair are close to each other. It seems

interesting in this connection to perform the light front analysis of the GSI, AGS and SPS data.

4. CONCLUSIONS

The light front analysis of π^- – mesons in the relativistic nucleus-nucleus collisions is carried out. The results of this paper confirm the conclusions of our previous publication [1], that the phase space of secondary π^- mesons is divided into two parts, in one of which the thermal equilibrium seems to be reached. Corresponding temperatures are obtained from the fitting of the data by the Boltzmann distribution. The characteristics of the π^- mesons (the momentum, angular, p_T^2 – distributions) in these two regions differ significantly. The dependence of T on $(A_P * A_T)^{1/2}$ has been studied. The temperature decreases with increase of $(A_P * A_T)^{1/2}$. The experimental results have been compared with the QGSM. The model seems to be in a good agreement with the data excluding O-Pb collisions – the heaviest colliding pair.

ACKNOWLEDGEMENTS

The authors express their deep gratitude to J.-P.Alard, Sh.Esakia, D.Ferenc, G.Kuratashvili, J.-F.Mathiot, Z.Menteshashvili, G.Paic for interesting discussions.

References

- [1] M.Anikina et al., Nucl.Phys. A640 (1998) 111;
N.Amaglobeli, V.Garsevanishvili et al., Eur.Phys. J. C8 (1999) 603
- [2] M.Anikina et al., Phys.Rev. C33 (1986) 895
- [3] M.Anikina et al., JINR Report E1-84-785,Dubna (1984) 17
- [4] P.A.M.Dirac, Rev.Mod.Phys. 21 (1949) 392
- [5] V.Garsevanishvili, A.Kvinikhidze, V.Matveev, A.Tavkhelidze, R.Faustov Sov. J. Theor. and Math.Phys. 23 (1975) 310
- [6] S.J.Chang, R.G.Root, T.M.Yan Phys.Rev. D7 (1973) 1133
- [7] H.Leutwyler, Nucl.Phys. B76 (1974) 413
- [8] S.J.Brodsky, G.McCartor, H.C.Pauli, S.S.Pinsky. Particle World 3 (1993) 109
- [9] K.G.Wilson, T.S.Walout, A.Harindranath, W.M.Zhang, R.J.Perry, St.D.Glazek Phys.Rev. D49 (1994) 6720
- [10] B.Desplanques, V.A.Karmanov, J.F.Mathiot Nucl.Phys. A589 (1995) 697;
J.Carbonell, B.Desplanques, V.A.Karmanov, J.F.Mathiot. To appear in Phys. Rep.
- [11] E.L.Feinberg, Sov. J. Uspekhi Fiz. Nauk, 164 (1971) 539
- [12] J.Gunion, SLAC-PUB-2607, September, 1980
- [13] N.Amelin et al., Phys.Rev.Lett. 67 (1991) 1523
- [14] B.Andersson, G Gustafsson and B.Nilsson-Almqvist, Nucl.Phys. B281 (1987) 289
- [15] N.Amelin and L.Csernai, In Proc. of the Int. Workshop on Correlations and Multi-particle Production (CAMP), Marburg, Germany, 1990 (World Scientific, Singapore, 1990);
N.Amelin, K.Gudima and V.Toneev, Sov.J. Nucl.Phys. 51 (1990) 327
- [16] L.Chkhaidze et al., Eur. Phys.J. A1 (1998) 299

- [17] L.Bravina, N.Amelin, L.Csernai, P.Levai and D.Strottman, Nucl.Phys A566 (1994) 376
- [18] L.Chkhaidze et al., Z.Phys. C54 (1992) 179
- [19] P.Baltes et al., GSI Scientific Report 92-1, (1992) 50;
L.Venema et al., GSI Scientific Report 92-1, Darmstadt (1992) 42;
M.Pfeiffer et al., GSI Scientific Report 93-1, Darmstadt (1993) 58;
M.Appenheimer al., GSI Scientific Report 97-1,Darmstadt (1997) 58
- [20] N.Herrmann Nucl.Phys. A610 (1996) 49c

FIGURE CAPTIONS

Fig. 1 The ξ^\pm – distribution of π^- mesons a) from $\ast - \text{He}(\text{Li}, \text{C})$, $\triangle - \text{C-Ne}$, $\circ - \text{O-Pb}$ interactions. b) From C-Cu interactions: $\circ -$ the experimental data, $\triangle -$ the QGSM data.

The curves are the result of polynomial approximation of the experimental data.

Fig. 2 The x_F – distribution of π^- mesons from $\ast - \text{He}(\text{Li}, \text{C})$, $\triangle - \text{C-Cu}$, $\circ - \text{O-Pb}$ interactions.

Fig. 3 The ζ^\pm – distribution of π^- mesons a) from $\ast - \text{He}(\text{Li}, \text{C})$, $\triangle - \text{C-Ne}$, $\circ - \text{O-Pb}$ interactions. b) From C-Cu interactions: $\circ -$ the experimental data, $\triangle -$ the QGSM data.

The curves are the result of polynomial approximation of the experimental data.

Fig. 4 The p_T^2 distribution of π^- mesons from $\ast - \text{He}(\text{Li}, \text{C})$, $\triangle - \text{C-Ne}$, $\circ - \text{O-Pb}$ interactions a) for $\zeta^+ > \tilde{\zeta}^+$. b) For $\zeta^+ < \tilde{\zeta}^+$. c) From C-Cu interactions for $\zeta^+ > \tilde{\zeta}^+$ $\circ -$ experimental and $\triangle -$ the QGSM data; for $\zeta^+ < \tilde{\zeta}^+$ $\square -$ experimental and $\ast -$ the QGSM data.

The solid lines - fit of the experimental data in the regions $\zeta^+ > \tilde{\zeta}^+$ and $\zeta^+ < \tilde{\zeta}^+$ by the Eqs.(5) and (8), correspondingly.

Fig. 5 The $\cos\Theta$ distribution of π^- mesons from $\ast - \text{He}(\text{Li}, \text{C})$, $\triangle - \text{C-Ne}$, $\circ - \text{O-Pb}$ interactions a) for $\zeta^+ > \tilde{\zeta}^+$. b) For $\zeta^+ < \tilde{\zeta}^+$. c) From C-Cu interactions for $\zeta^+ > \tilde{\zeta}^+$ $\circ -$ experimental and $\triangle -$ the QGSM data; for $\zeta^+ < \tilde{\zeta}^+$, $\square -$ experimental and $\ast -$ the QGSM data.

The solid lines - fit of the experimental data in the region $\zeta^+ > \tilde{\zeta}^+$ by the Eq.(6) and in the $\zeta^+ < \tilde{\zeta}^+$ by the polynom.

Fig. 6 The momentum distribution of π^- mesons from C-Cu interactions in the laboratory system. The shaded area corresponds to the region of $\zeta^+ > \tilde{\zeta}^+$.

Fig. 7 The dependence of $\langle P \rangle_{lab}$ on Θ_{lab} in the regions $\zeta^+ > \tilde{\zeta}^+$ (bottom data) and $\zeta^+ < \tilde{\zeta}^+$ (top data) for $\square - \text{He}(\text{Li}, \text{C})$ and C-Ne, $\diamond - \text{C-Cu}$, $\ast - \text{Mg-Mg}$, $\circ - \text{O-Pb}$. The curves – result of polynomial approximation.

Fig. 8 The $(1/\pi) \cdot dN/d\zeta^+$ distribution of π^- mesons from C-Cu interactions. \circ – experimental data, the solid line – fit of the experimental data in the region $\zeta^+ > \tilde{\zeta}^+$ by the Eq.(4), the dashed line – fit of the experimental data in the region $\zeta^+ < \tilde{\zeta}^+$ by the Eq.(9).

Fig. 9 The dependence of the parameter T on $(A_P * A_T)^{1/2}$ for He(Li,C), C-Ne, Mg-Mg, C-Cu and O-Pb. \circ – the experimental data, \triangle – the QGSM data. The dashed line is a result of linear approximation of the experimental data.

TABLE CAPTIONS

Table 1. Number of the events, trigger and the results of the joint fit of the distributions $1/\pi \cdot dN/d\zeta^+$, dN/dp_T^2 , $dN/d\cos\Theta$ of π^- – mesons by Eqs. (4), (5), (6) in the region $\zeta^+ > \tilde{\zeta}^+$ and $1/\pi \cdot dN/d\zeta^+$ distributions by Eq.(9) in the region $\zeta^+ < \tilde{\zeta}^+$.

Table 1. Number of the events, trigger and the results of the joint fit of the distributions $1/\pi \cdot dN/d\zeta^+$, dN/dp_T^2 , $dN/d\cos\Theta$ of π^- – mesons by Eq. (4), (5), (6) in the region $\zeta^+ > \tilde{\zeta}^+$ and $1/\pi \cdot dN/d\zeta^+$ distributions by Eq.(9) in the region $\zeta^+ < \tilde{\zeta}^+$.

$A_p - A_T$ $T(\Theta_{ch}, \Theta_n)$		Number of events	T (MeV) $\zeta^+ > \tilde{\zeta}^+$	n $\zeta^+ < \tilde{\zeta}^+$
$He(Li, C)$ $T(2, 0)$	exp.	6147	81 ± 2	3.6 ± 0.2
	QGSM	15566	84 ± 2	3.5 ± 0.1
$C - Ne$ $T(2, 0)$	exp.	902	79 ± 3	3.7 ± 0.2
	QGSM	3950	82 ± 2	3.4 ± 0.8
$C - Cu$ $T(3, 3)$	exp.	1203	72 ± 2	3.0 ± 0.1
	QGSM	3463	74 ± 2	3.2 ± 0.8
$O - Pb$	exp.	732	55 ± 3	2.6 ± 0.1

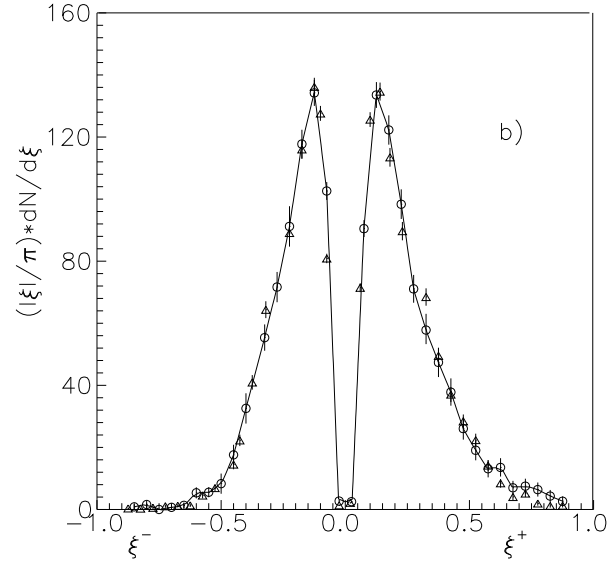
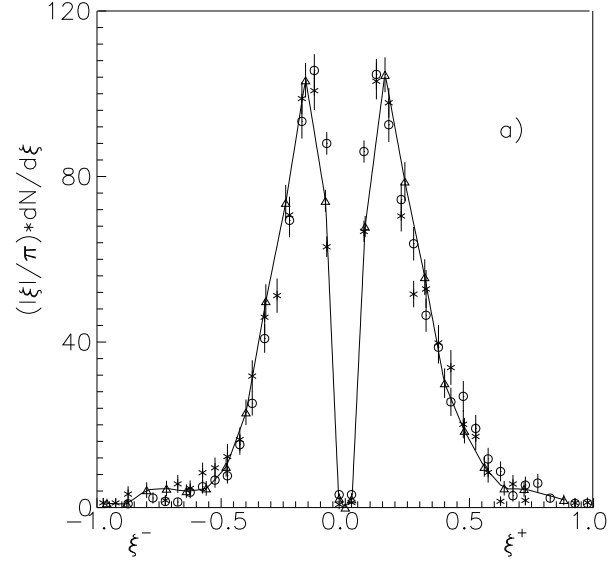


Figure 1: The ξ^\pm – distribution of π^- mesons a) from $* - \text{He}(\text{Li}, \text{C})$, $\triangle - \text{C-Ne}$, $\circ - \text{O-Pb}$ interactions. b) From C-Cu interactions: \circ – the experimental data, \triangle – the QGSM data. The curves are the result of polynomial approximation of the experimental data.

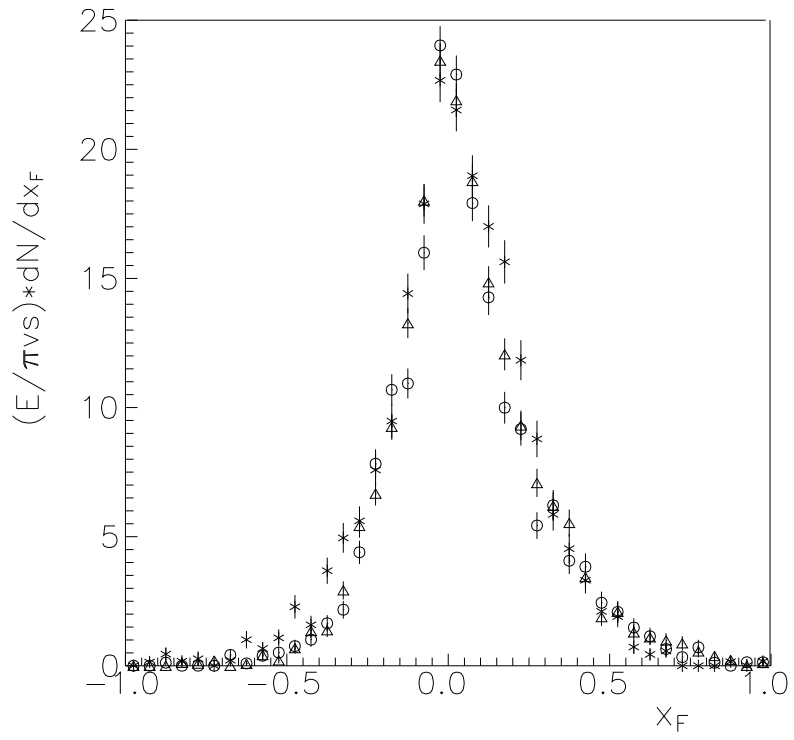


Figure 2: The x_F – distribution of π^- mesons from * – He(Li,C), Δ – C-Cu, o – O-Pb interactions.

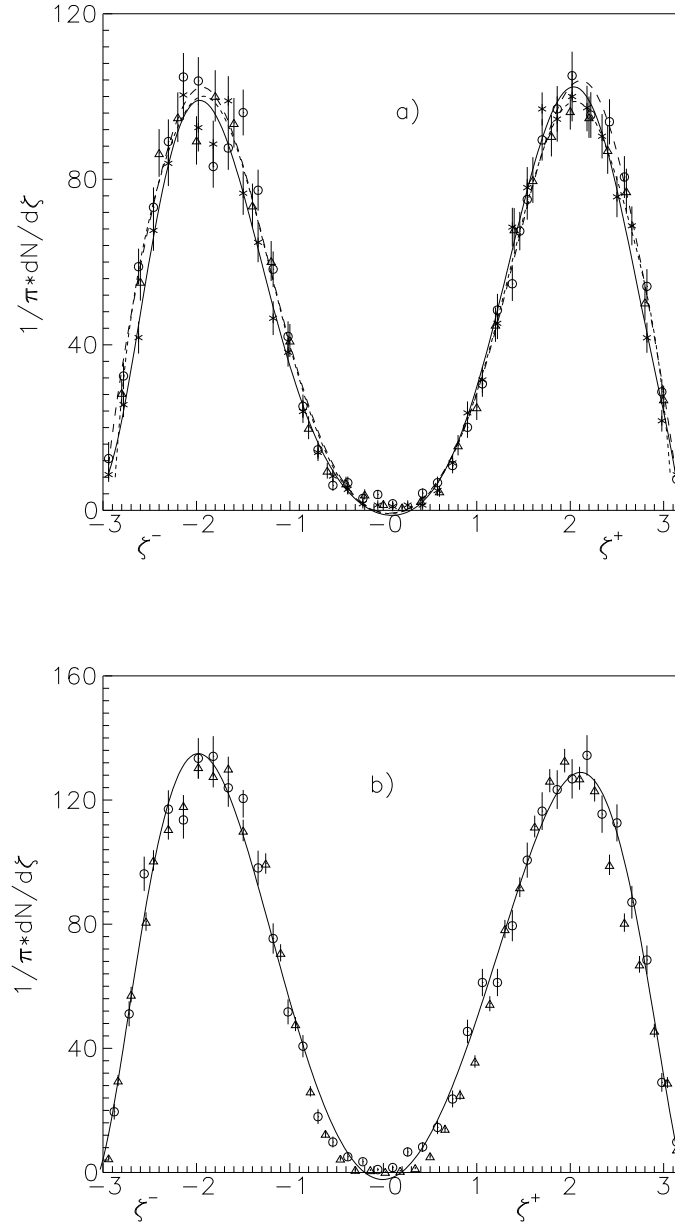


Figure 3: The ζ^\pm – distribution of π^- mesons a) from $* - \text{He}(\text{Li}, \text{C})$, $\Delta - \text{C-Ne}$, $\circ - \text{O-Pb}$ interactions. b) From C-Cu interactions: \circ – the experimental data, Δ – the QGSM data. The curves are the result of polynomial approximation of the experimental data.

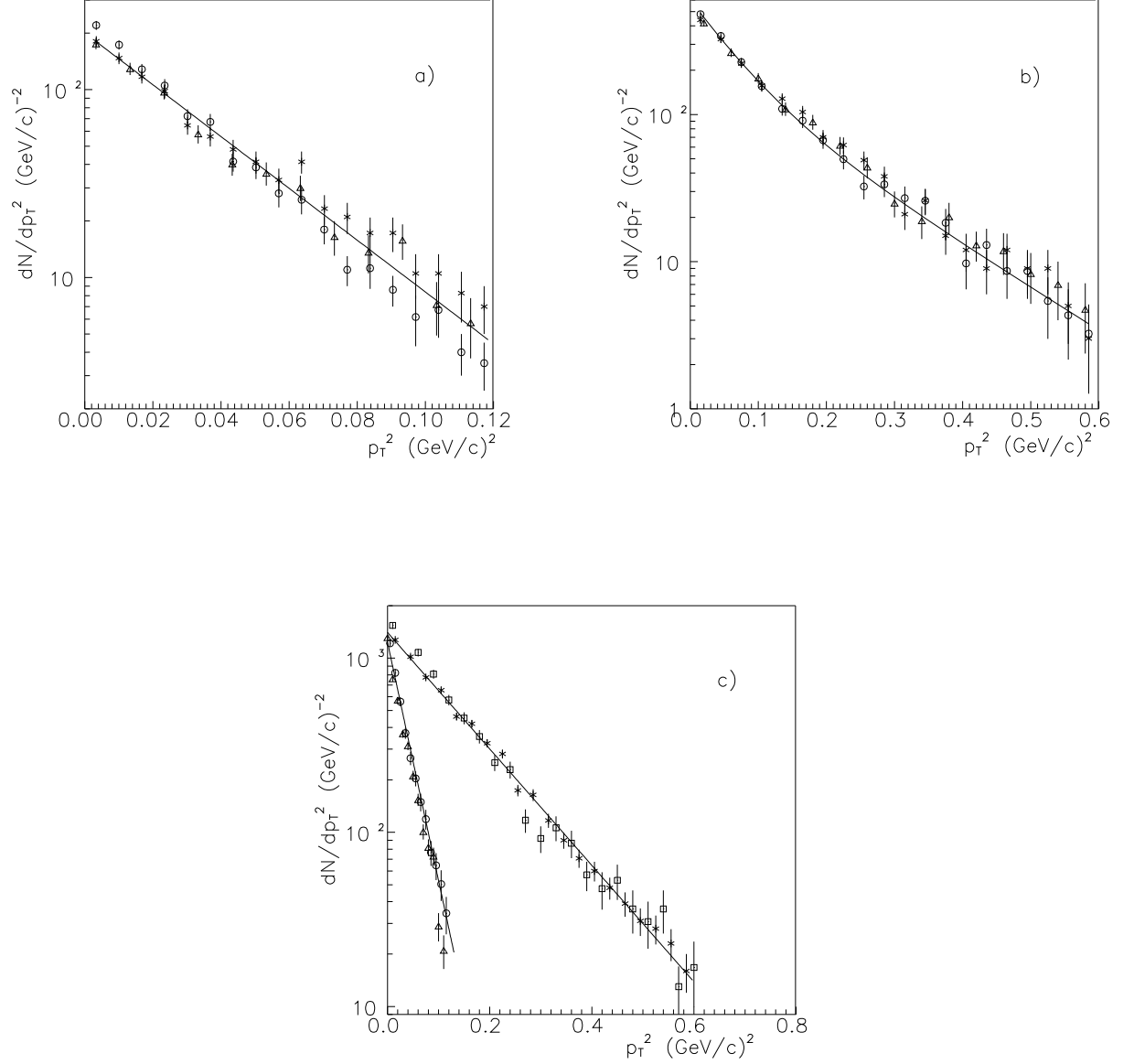


Figure 4: The p_T^2 distribution of π^- mesons from $*$ – He(Li,C), Δ – C-Ne, \circ – O-Pb interactions a) for $\zeta^+ > \tilde{\zeta}^+$. b) For $\zeta^+ < \tilde{\zeta}^+$. c) From C-Cu interactions for $\zeta^+ > \tilde{\zeta}^+$ \circ – experimental and Δ – the QGSM data; for $\zeta^+ < \tilde{\zeta}^+$ \square – experimental and $*$ – the QGSM data. The solid lines - fit of the experimental data in the regions $\zeta^+ > \tilde{\zeta}^+$ and $\zeta^+ < \tilde{\zeta}^+$ by the Eqs.(5) and (8), correspondingly.

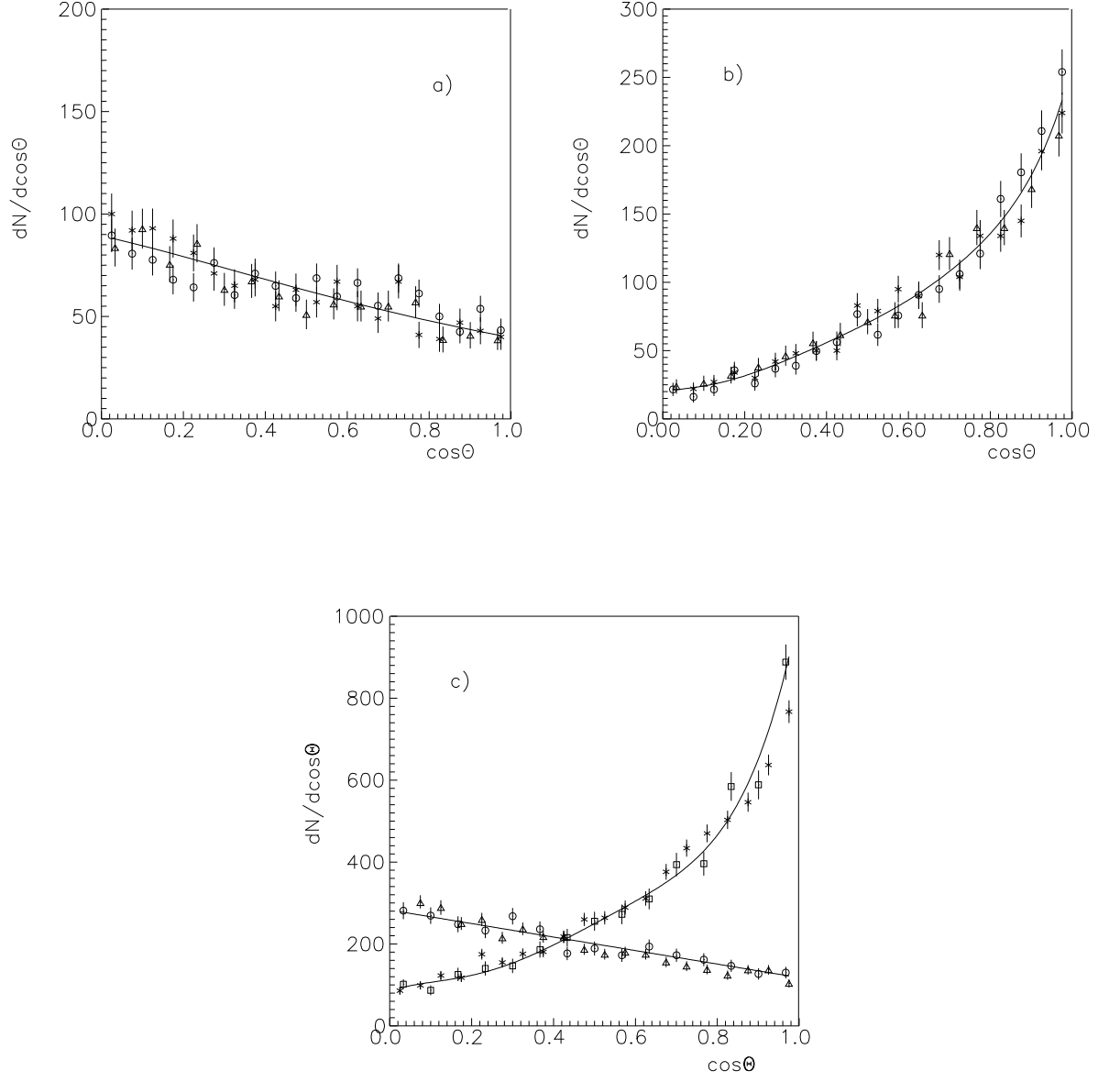


Figure 5: The $\cos\Theta$ distribution of π^- mesons from * – He(Li,C), Δ – C-Ne, \circ – O-Pb interactions a) for $\zeta^+ > \tilde{\zeta}^+$. b) For $\zeta^+ < \tilde{\zeta}^+$. c) From C-Cu interactions for $\zeta^+ > \tilde{\zeta}^+$ \circ – experimental and Δ – the QGSM data; for $\zeta^+ < \tilde{\zeta}^+$ \square – experimental and * – the QGSM data. The solid lines - fit of the experimental data in the region $\zeta^+ > \tilde{\zeta}^+$ by the Eq.(6) and in the $\zeta^+ < \tilde{\zeta}^+$ by the polynomial.

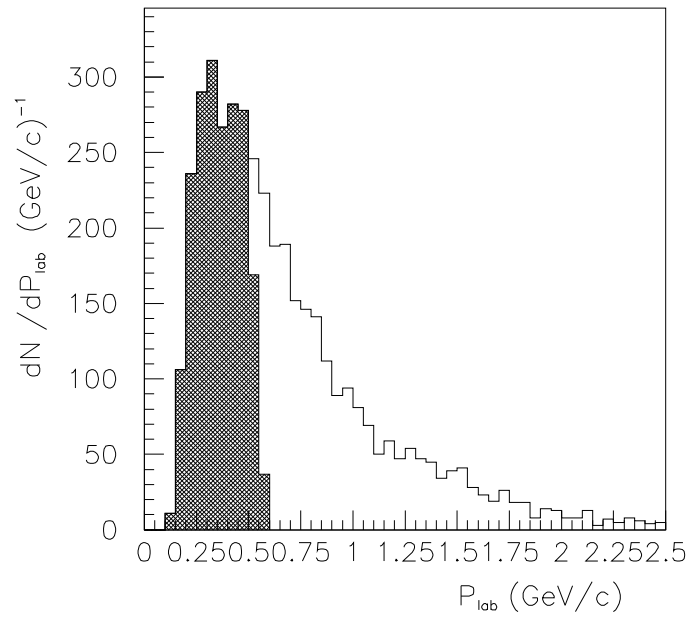


Figure 6: The momentum distribution of π^- mesons from C-Cu interactions in the laboratory system. The shaded area corresponds to the region of $\zeta^+ > \tilde{\zeta}^+$.

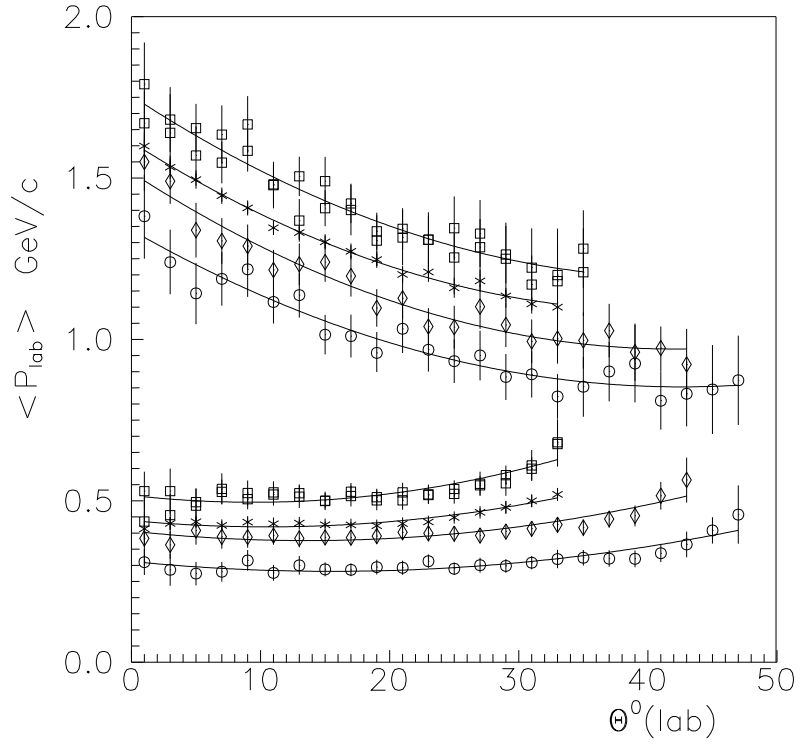


Figure 7: The dependence of $\langle P \rangle_{lab}$ on Θ_{lab} in the regions $\zeta^+ > \tilde{\zeta}^+$ (bottom data) and $\zeta^+ < \tilde{\zeta}^+$ (top data) for \square – He(Li,C) and C-Ne, \diamond – C-Cu, $*$ – Mg-Mg, \circ – O-Pb. The curves – result of polynomial approximation.

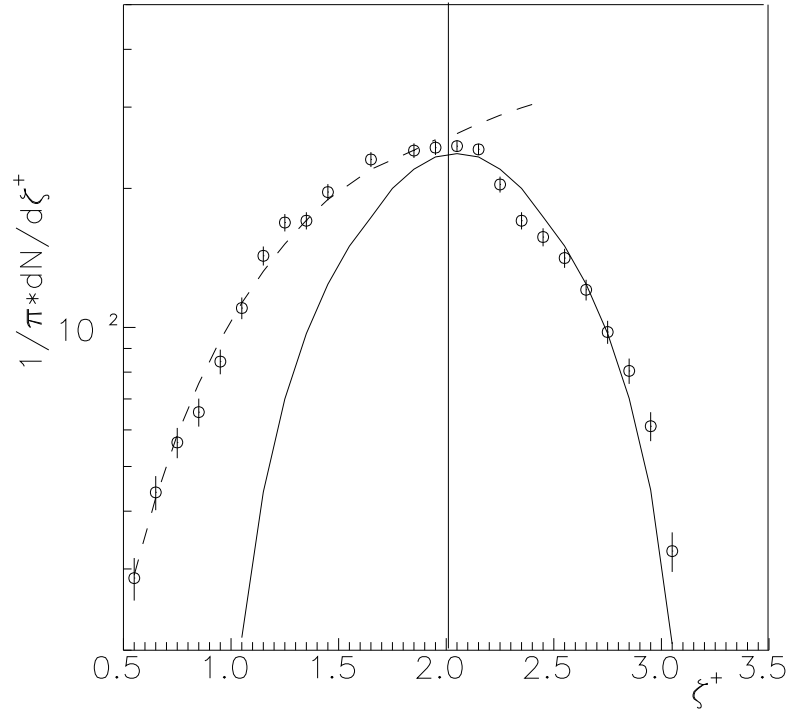


Figure 8: The $(1/\pi) \cdot dN/d\zeta^+$ distribution of π^- mesons from C-Cu interactions. \circ – experimental data, the solid line – fit of the experimental data in the region $\zeta^+ > \zeta^+_{\tilde{}}$ by the Eq.(4), the dashed line – fit of the experimental data in the region $\zeta^+ < \zeta^+_{\tilde{}}$ by the Eq.(9).

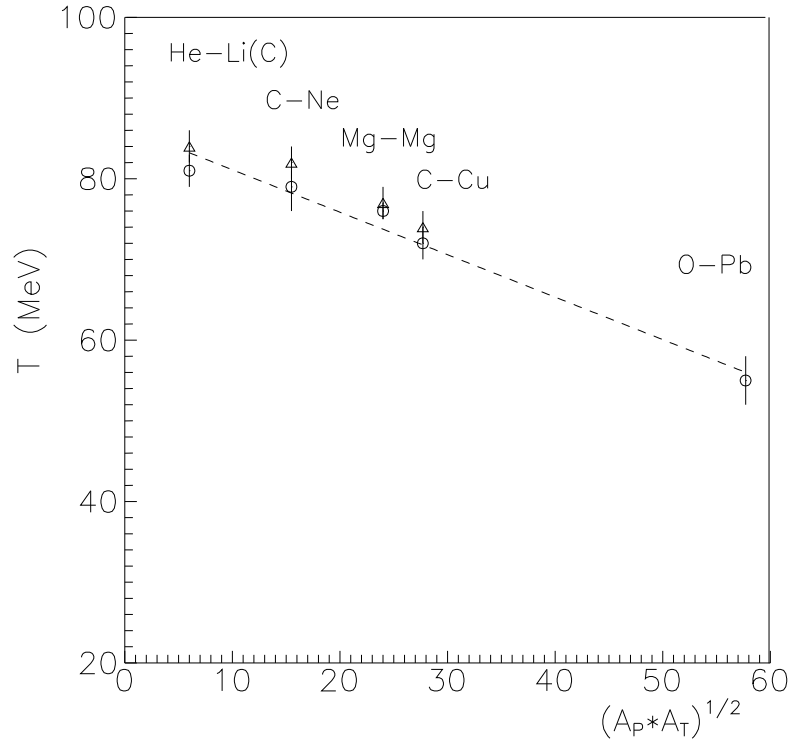


Figure 9: The dependence of the parameter T on $(A_P * A_T)^{1/2}$ for He(Li,C), C-Ne, Mg-Mg, C-Cu and O-Pb. \circ – the experimental data, \triangle – the QGSM data. The dashed line is a result of linear approximation.